Journal of Engineering Mathematics **49:** 253–270, 2004.

Influence functions of a point source for perforated compound plates with facial convection

Y.A. MELNIKOV
Department of Mathematical Sciences, Middle Tennessee State University, Murfreesboro, Tennessee 37132, U.S.A.

Received 11 November 2003; accepted in revised form 18 March 2004

Abstract. Steady-state heat conduction is considered for perforated thin plates with non-insulated facial surfaces. The heat conductivities of the materials and the convection coefficients are assumed piecewise constant. Influence functions of point sources are analytically obtained for some such plates of standard shape. Their singular components are derived in a closed form, ensuring accurate straightforward computer implementations. Special integral representations are then used for obtaining influence functions of a point source for perforated plates. Computability of those representations is tested with a number of illustrative examples.

Key words: Green's functions, non-insulated facial surfaces, steady-state heat conduction, thin perforated plates

1. Introduction

Although the influence (Green's) function-based methods are proven to be productive [1–6] in solving certain problem classes in applied mechanics, an extensive employment of these methods in engineering science is still limited and is not commensurate with their potential power. One of the reasons that keeps the engineering community hesitant about the wide use of these methods is a lack of readily computable representations of influence functions of a point source in literature. This observation has motivated the author's involvement in the present project.

As it is known [7, Chapter 4], the Green's function of the Dirichlet problem for Laplace's equation over a simply connected region D can be written as

$$G(z,\zeta) = \frac{1}{2\pi}\log\left|\frac{1-w(z)\overline{w(\zeta)}}{w(z)-w(\zeta)}\right|,$$

where $w(z)$ represents a complex-variable function that delivers conformal mapping of D onto the interior of the unit circle, with z and ζ standing for the observation and the source point, respectively, and where the bar on $w(\zeta)$ denotes the complex conjugate. Note that only for a few regions of standard shape, $w(z)$ represents an elementary function. That is why influence functions of a point source, even for thin plates made of a homogeneous isotropic material, with the facial surfaces insulated, are available in closed form only for a few standard plate configurations, such as half-plane, infinite wedge, circle, circular sector, infinite, and semi-infinite strip.

For a much broader set of plate configurations and boundary conditions different from the Dirichlet type, influence functions are constructible in a series form like, for instance, the classical double Fourier-series expansion for a rectangular plate. Note however that, as

to numerical implementations, a series appearance of influence functions has a notable drawback. Indeed, such series do not converge uniformly because of the singularity of influence functions.

Clearly, the convergence rate of series expansions of influence functions is reduced if the latter is differentiated, which is always a necessity in numerical procedures that are based on influence-function-based methods, as some versions of the boundary-element method, for example. Work towards increasing the practicality of influence functions has resulted in notable progress in the past decades [8–10] in improving the convergence rate of series representations of such functions. In this regard a brief comment is appropriate. The author of [10] failed to cite very similar work on the subject (see, for example, [8]) that was published much earlier.

In this study we aim at obtaining some readily computable representations of influence functions of a point source for perforated thin plates with non-insulated facial surfaces and with piecewise constant heat conductivities of the materials of which the plates are made. To outline the novelty of this study, we refer the reader to the recent benchmark monograph [4, Chapter 5] that analyzes the status quo and reviews current trends in the field of applications of Green's functions. Note also that, although Green's functions have recently [5, 6] been constructed for some advanced material (inhomogeneous and anisotropic) systems, so far there has not been proposed an approach for obtaining such functions for multiply connected regions of complex configuration filled with piecewise homogeneous materials to which the present work is, in fact, devoted.

2. Plates of standard shape

The technique proposed earlier [2, Chapter 7] for an analytical construction of Green's functions for potential problems posed on compound regions, is extended, in this section, to some steady-state heat-conduction problems for compound plates of standard configuration with non-insulated facial surfaces.

2.1. Infinite strip-shaped plate

Let a thin plate, whose middle plane occupies an infinite strip-shaped region D, be composed of two fragments $D_1 = \{-\infty < x < 0,\ 0 < y < b\}$ and $D_2 = \{0 < x < \infty,\ 0 < y < b\}$, each of which is made of a homogeneous isotropic material, with λ_1 and λ_2 representing their coefficients of heat conduction. Consider the boundary-contact-value problem

$$u_i(x, 0) = u_i(x, b) = 0, \tag{1}$$

$$|u_1(-\infty, y)| < \infty, \quad |u_2(\infty, y)| < \infty, \tag{2}$$

$$u_1(0, y) = u_2(0, y), \quad \frac{\partial u_1(0, y)}{\partial x} = \lambda \frac{\partial u_2(0, y)}{\partial x} \tag{3}$$

defined on D for the so-called [11, Chapter 9] *static Klein-Gordon* equation

$$\nabla^2 u_i(x, y) - k_i^2 u_i(x, y) = -f_i(x, y), \quad (x, y) \in D_i, \quad i = 1, 2, \tag{4}$$

where $\lambda = \lambda_2/\lambda_1$, ∇^2 is the Laplace operator, and the parameters k_i^2 are directly proportional to the convection coefficients through the plate's facial surfaces.

The $k_i^2 u_i(x, y)$ term in Equation (4) simulates the Newtonian convection through the plate's facial surfaces. The case of insulated faces results in $k_i^2 = 0$ and the governing equation (4) reduces to the standard Laplace form.

To obtain an analytic form of the influence function of a point source for the plate, we expand the functions $u_i(x, y)$ and $f_i(x, y)$ in Fourier series

$$u_i(x, y) = \sum_{n=1}^{\infty} u_{i,n}(x) \sin(\nu y), \qquad \nu = \frac{n\pi}{b}, \quad i = 1, 2 \tag{5}$$

and

$$f_i(x, y) = \sum_{n=1}^{\infty} f_{i,n}(x) \sin(\nu y), \qquad i = 1, 2 \tag{6}$$

and substitute these in Equatons (1–4). This yields the following three-point boundary-contact-value problem

$$\frac{\mathrm{d}^2 u_{1,n}(x)}{\mathrm{d}x^2} - (\nu^2 + k_1^2) u_{1,n}(x) = -f_{1,n}(x), \qquad x \in (-\infty, 0), \tag{7}$$

$$\frac{\mathrm{d}^2 u_{2,n}(x)}{\mathrm{d}x^2} - (\nu^2 + k_2^2) u_{2,n}(x) = -f_{2,n}(x), \qquad x \in (0, \infty), \tag{8}$$

$$|u_{1,n}(-\infty)| < \infty, \quad |u_{2,n}(\infty)| < \infty, \tag{9}$$

$$u_{1,n}(0) = u_{2,n}(0), \quad \frac{\mathrm{d}u_{1,n}(0)}{\mathrm{d}x} = \lambda \frac{\mathrm{d}u_{2,n}(0)}{\mathrm{d}x} \tag{10}$$

in the coefficients of the expansion in Equation (5). With the method of variation of parameters in hand, the solution to the above setting is obtained as

$$u_{1,n}(x) = \frac{1}{2h_1} \int_{-\infty}^{x} \left[\mathrm{e}^{-h_1(x-\xi)} - \mathrm{e}^{h_1(x-\xi)}\right] f_{1,n}(\xi)\mathrm{d}\xi$$

$$+ \int_{-\infty}^{0} \frac{(h_1 - \lambda h_2)\mathrm{e}^{h_1(x+\xi)} + (h_1 + \lambda h_2)\mathrm{e}^{h_1(x-\xi)}}{2h_1(h_1 + \lambda h_2)} f_{1,n}(\xi)\mathrm{d}\xi + \int_{0}^{\infty} \frac{\lambda}{h_1 + \lambda h_2} \mathrm{e}^{h_1 x - h_2 \xi} f_{2,n}(\xi)\mathrm{d}\xi$$

and

$$u_{2,n}(x) = \frac{1}{2h_2} \int_{0}^{x} \left[\mathrm{e}^{-h_2(x-\xi)} - \mathrm{e}^{h_2(x-\xi)}\right] f_{2,n}(\xi)\mathrm{d}\xi + \int_{-\infty}^{0} \frac{1}{h_1 + \lambda h_2} \mathrm{e}^{h_1 x - h_2 \xi} f_{1,n}(\xi)\mathrm{d}\xi$$

$$+ \int_{0}^{\infty} \frac{(h_1 + \lambda h_2)\mathrm{e}^{h_2(x-\xi)} - (h_1 - \lambda h_2)\mathrm{e}^{-h_2(x+\xi)}}{2h_1(h_1 + \lambda h_2)} f_{2,n}(\xi)\mathrm{d}\xi,$$

where $h_i = \sqrt{\nu^2 + k_i^2}$, $(i = 1, 2)$.

We rewrite these in a compact form as

$$u_{1,n}(x) = \int_{-\infty}^{0} g_{11}^{n}(x, \xi) f_{1,n}(\xi)\mathrm{d}\xi + \int_{0}^{\infty} g_{12}^{n}(x, \xi) f_{2,n}(\xi)\mathrm{d}\xi \tag{11}$$

and

$$u_{1,n}(x) = \int_{-\infty}^{0} g_{21}^{n}(x,\xi)\, f_{1,n}(\xi)\mathrm{d}\xi + \int_{0}^{\infty} g_{22}^{n}(x,\xi)\, f_{2,n}(\xi)\mathrm{d}\xi, \tag{12}$$

where the kernel functions $g_{ij}^{n}(x,\xi)$ are expressed as

$$g_{11}^{n}(x,\xi) = \frac{(h_1+\lambda h_2)\mathrm{e}^{-h_1|x-\xi|} + (h_1-\lambda h_2)\mathrm{e}^{h_1(x+\xi)}}{2h_1(h_1+\lambda h_2)} \tag{13}$$

with both variables x and ξ belonging to the segment $(-\infty, 0]$,

$$g_{12}^{n}(x,\xi) = \frac{\lambda}{h_1+\lambda h_2}\mathrm{e}^{h_1 x - h_2 \xi}, \quad -\infty < x \le 0, \quad 0 \le \xi < \infty,$$

$$g_{21}^{n}(x,\xi) = \frac{1}{h_1+\lambda h_2}\mathrm{e}^{h_1 x - h_2 \xi}, \quad 0 \le x < \infty, \quad -\infty < \xi \le 0$$

and

$$g_{22}^{n}(x,\xi) = \frac{(h_1+\lambda h_2)\mathrm{e}^{-h_2|x-\xi|} - (h_1-\lambda h_2)\mathrm{e}^{-h_2(x+\xi)}}{2h_2(h_1+\lambda h_2)} \tag{14}$$

with both variables x and ξ belonging to the segment $[0, \infty)$.

Clearly, the coefficients $f_{i,n}(\xi)$ of the expansions in Equation (6) can be expressed in terms of the right-hand-side functions $f_i(\xi,\eta)$ of Equation (4) as

$$f_{i,n}(\xi) = \frac{2}{b}\int_{0}^{\pi} f_i(\xi,\eta)\sin(\nu\eta)\mathrm{d}\eta, \quad i = 1, 2.$$

By substituting these in Equations (11) and (12) and then in Equation (5), one obtains the solution to the problem in (1–4) in the form

$$u_i(x,y) = \int_{0}^{\pi}\int_{-\infty}^{0}\left(\frac{2}{b}\sum_{n=1}^{\infty} g_{i1}^{n}(x,\xi)\sin(\nu y)\sin(\nu\eta)\right) f_1(\xi,\eta)\mathrm{d}\xi\,\mathrm{d}\eta$$

$$+\int_{0}^{\pi}\int_{0}^{\infty}\left(\frac{2}{b}\sum_{n=1}^{\infty} g_{i2}^{n}(x,\xi)\sin(\nu y)\sin(\nu\eta)\right) f_2(\xi,\eta)\mathrm{d}\xi\,\mathrm{d}\eta, \quad (x,y)\in D_i.$$

Thus, the kernels

$$G_{ij}(x,y;\xi,\eta) = \frac{2}{b}\sum_{n=1}^{\infty} g_{ij}^{n}(x,\xi)\sin(\nu y)\sin(\nu\eta) \tag{15}$$

of the above representation for $u_i(x,y)$ determine the influence function of a point source that we are looking for. It is important to note that the subscripts in $G_{ij}(x,y;\xi,\eta)$ specify the subregions of D to which the observation and the source point belong. That is, $(x,y)\in D_i$ and $(\xi,\eta)\in D_j$.

Note that, in dealing with influence functions for compound regions of the kind considered in this study, it is convenient to use a notion of the *matrix of Green's type* that has

been introduced in our earlier works [2, Chapter 7]. This notion most adequately reflects the matrix format of influence functions for compound regions. Accordingly, the functions $G_{ij}(x, y; \xi, \eta)$ will be referred to, in what follows, as the entries of the matrix of Green's type of the boundary-contact-value problem posed with Equations (1–4).

2.1.1. *Splitting off the singular component*

The fundamental solution for the static Klein-Gordon equation in two dimensions yields the same logarithmic-type singularity as the Laplace equation has. This causes for the series in (15) not to converge uniformly for the main diagonal entries of the matrix of Green's type, whereas it converges uniformly for the other two entries.

A special approach is used herein as suggested in [8] to split off the singular components of $G_{11}(x, y; \xi, \eta)$ and $G_{22}(x, y; \xi, \eta)$ and to accelerate the convergence rate of the series representing the regular components.

From the analysis of the series in (15), it follows that the singularity of the entries $G_{11}(x, y; \xi, \eta)$ and $G_{22}(x, y; \xi, \eta)$ is associated with the first exponential terms of the coefficients $g^n_{11}(x, \xi)$ and $g^n_{22}(x, \xi)$ (see Equations (13) and (14)). Recalling the coefficient $g^n_{11}(x, \xi)$, for example, we isolate first the singularity containing term in $G_{11}(x, y; \xi, \eta)$

$$G_{11}(x, y; \xi, \eta) = \frac{1}{b}\sum_{n=1}^{\infty}\frac{e^{-h_1|x-\xi|}}{h_1}\sin(\nu y)\sin(\nu\eta)$$

$$+\frac{1}{b}\sum_{n=1}^{\infty}\frac{(h_1-\lambda h_2)e^{h_1(x+\xi)}}{h_1(h_1+\lambda h_2)}\sin(\nu y)\sin(\nu\eta) \tag{16}$$

and then apply the following transformation to it

$$\frac{1}{b}\sum_{n=1}^{\infty}\frac{e^{-h_1|x-\xi|}}{h_1}\sin(\nu y)\sin(\nu\eta) = \frac{1}{b}\sum_{n=1}^{\infty}\left[\frac{e^{-h_1|x-\xi|}}{h_1} - \frac{e^{-\nu|x-\xi|}}{\nu}\right]\sin(\nu y)\sin(\nu\eta).$$

$$+\frac{1}{b}\sum_{n=1}^{\infty}\frac{e^{-\nu|x-\xi|}}{\nu}\sin(\nu y)\sin(\nu\eta) \tag{17}$$

It can readily be shown that the first of the above two series converges uniformly for any interior location of the source and the observation point. To justify this statement, we evaluate the modulus of its N-th remainder

$$|R_N(x, y; \xi, \eta)| = \left|\sum_{n=N+1}^{\infty}\left[\frac{e^{-\nu|x-\xi|}}{\nu} - \frac{e^{-h_1|x-\xi|}}{h_1}\right]\sin(\nu y)\sin(\nu\eta)\right|$$

$$\leq \sum_{n=N+1}^{\infty}\frac{h_1 e^{-\nu|x-\xi|} - \nu e^{-h_1|x-\xi|}}{\nu h_1} < \sum_{n=N+1}^{\infty}\frac{h_1 e^{-\nu|x-\xi|} - \nu e^{-h_1|x-\xi|}}{\nu^2}.$$

Since values of the parameter $h_1 = \sqrt{\nu^2 + k_1^2}$ never exceed the quantity of $\nu + k_1$ (the triangle inequality), the above estimation can further be developed as

$$|R_N(x, y; \xi, \eta)| < \sum_{n=N+1}^{\infty}\frac{1}{\nu^2}[(\nu+k_1)e^{-\nu|x-\xi|} - \nu e^{-(\nu+k_1)|x-\xi|}]$$

$$= [1-\mathrm{e}^{-k_1|x-\xi|}] \sum_{n=N+1}^{\infty} \frac{1}{\nu} \mathrm{e}^{-\nu|x-\xi|} + k_1 \sum_{n=N+1}^{\infty} \frac{1}{\nu^2} \mathrm{e}^{-\nu|x-\xi|}$$

$$\leq [1-\mathrm{e}^{-k_1|x-\xi|}] \sum_{n=N+1}^{\infty} \frac{1}{\nu} \mathrm{e}^{-\nu|x-\xi|} + k_1 \sum_{n=N+1}^{\infty} \frac{1}{\nu^2}$$

$$= \frac{b}{\pi}[1-\mathrm{e}^{-k_1|x-\xi|}] \left[\sum_{n=1}^{\infty} \frac{1}{n} \mathrm{e}^{-\frac{n\pi}{b}|x-\xi|} - \sum_{n=1}^{N} \frac{1}{n} \mathrm{e}^{-\frac{n\pi}{b}|x-\xi|} \right] + k_1 \frac{b^2}{\pi^2} \left[\sum_{n=1}^{\infty} \frac{1}{n^2} - \sum_{n=1}^{N} \frac{1}{n^2} \right].$$

Recalling standard summation formulas for the two infinite series in the above estimation, we complete the evaluation procedure for the remainder of the first series in (17) as

$$|R_N(x, y; \xi, \eta)| < \frac{b}{\pi} \left\{ [\mathrm{e}^{-k_1|x-\xi|} - 1] \left[\log \left(1 - \mathrm{e}^{-\frac{\pi}{b}|x-\xi|} \right) \right. \right.$$

$$\left. \left. + \sum_{n=1}^{N} \frac{1}{n} \mathrm{e}^{-\frac{n\pi}{b}|x-\xi|} \right] + k_1 \frac{b}{\pi} \left[\frac{\pi^2}{6} - \sum_{n=1}^{N} \frac{1}{n^2} \right] \right\}. \tag{18}$$

As it is clearly seen, the estimation we arrived at is not uniform. Indeed, it varies with the distance $d = |x-\xi|$ between the observation point and the source point. Let $U_N(d)$ be the right-hand side of the above inequality, representing the upper bound for $|R_N(x, y; \xi, \eta)|$. Figure 1 shows the graphs of the relative error

$$E(d) = \frac{10^3 \times U_N(d)}{\max \left| \sum_{n=1}^{\infty} \left[\frac{1}{h_1} \mathrm{e}^{-h_1|x-\xi|} - \frac{1}{\nu} \mathrm{e}^{-\nu|x-\xi|} \right] \sin(\nu y) \sin(\nu \eta) \right|}$$

for the first series in (17) computed for several values of the truncation parameter N (the parameter k_1 is fixed at the value of 0·1). Clearly, the error $E(d)$, being really small even at the immediate vicinity of the source point, rapidly goes to zero as d increases (even for $N = 25$). Figure 1 presents clear evidence of a uniform convergence of the first series in (17), which can subsequently be accurately computed by a direct truncation.

As to the second series of (17), it is not uniformly convergent. Indeed, it diverges when $(x, y) = (\xi, \eta)$ and its computability would be notably affected if the series is used in its current form. The situation can, however, be radically improved by a complete summation of that series, which yields

$$\frac{1}{b} \sum_{n=1}^{\infty} \frac{1}{\nu} \mathrm{e}^{-\nu|x-\xi|} \sin(\nu y) \sin(\nu \eta) = \frac{1}{2\pi} \log \frac{|\mathrm{e}^{\pi(z-\overline{\zeta})/b} - 1|}{|\mathrm{e}^{\pi(z-\zeta)/b} - 1|},$$

where z and ζ are again the observation and the source point, respectively. This results in a readily computable form for the first diagonal entry $G_{11}(x, y; \xi, \eta)$ of the matrix of Green's type. It is finally obtained as

$$G_{11}(x, y; \xi, \eta) = \frac{1}{2\pi} \log \frac{|\mathrm{e}^{\pi(z-\overline{\zeta})/b} - 1|}{|\mathrm{e}^{\pi(z-\zeta)/b} - 1|} + \frac{1}{b} \sum_{n=1}^{\infty} \left[\frac{\mathrm{e}^{-h_1|x-\xi|}}{h_1} - \frac{\mathrm{e}^{-\nu|x-\xi|}}{\nu} \right] \sin(\nu y) \sin(\nu \eta)$$

$$+ \frac{1}{b} \sum_{n=1}^{\infty} \frac{(h_1 - \lambda h_2) \mathrm{e}^{h_1(x+\xi)}}{h_1(h_1 + \lambda h_2)} \sin(\nu y) \sin(\nu \eta). \tag{19}$$

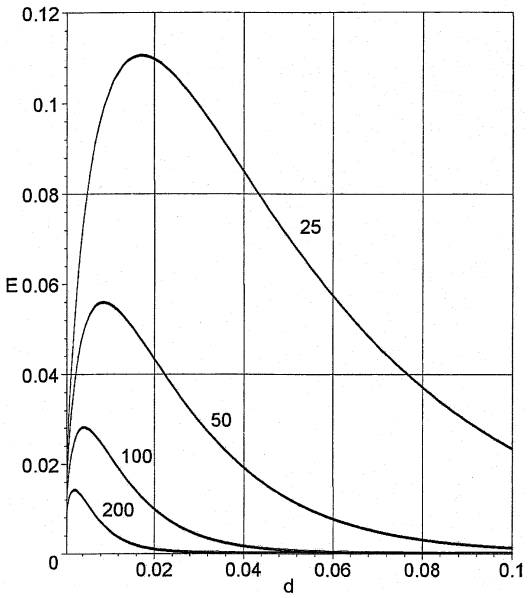

Figure 1. Relative error caused by truncation of the series in Equation (15).

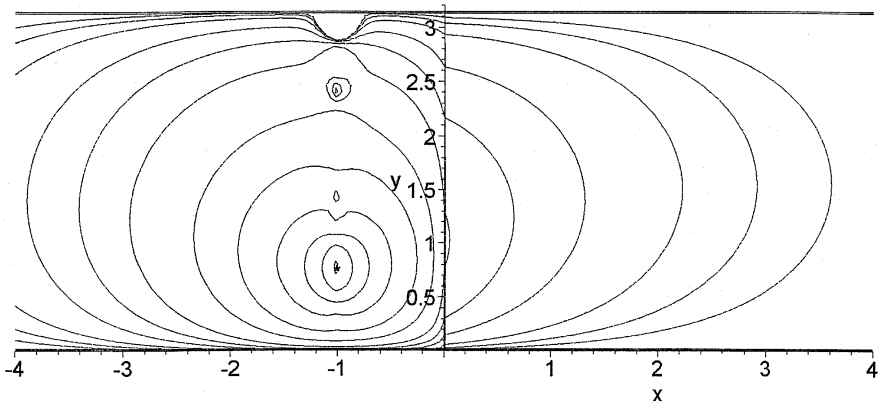

Figure 2. Profile of the influence function computed by truncation ($N = 20$) of the series in Equation (15).

For the second diagonal entry $G_{22}(x, y; \xi, \eta)$, we analogously obtain a computable form as

$$G_{22}(x, y; \xi, \eta) = \frac{1}{2\pi} \log \frac{|e^{\pi(z-\bar{\zeta})/b} - 1|}{|e^{\pi(z-\zeta)/b} - 1|} + \frac{1}{b} \sum_{n=1}^{\infty} \left[\frac{e^{-h_2|x-\xi|}}{h_2} - \frac{e^{-\nu|x-\xi|}}{\nu} \right] \sin(\nu y) \sin(\nu \eta)$$
$$+ \frac{1}{b} \sum_{n=1}^{\infty} \frac{(\lambda h_2 - h_1) e^{-h_1(x+\xi)}}{h_2(h_1 + \lambda h_2)} \sin(\nu y) \sin(\nu \eta). \tag{20}$$

To demonstrate the computational effect achieved by the splitting off of the singular terms in the diagonal entries of the matrix of Green's type, in Figures 2 and 3 we depicted the field generated by a unit source located at the point $(-1{\cdot}0, 0{\cdot}75)$ in D_1, with the rest of the parameters in the setting chosen as: $\lambda = 10$, $k_1 = 1{\cdot}0$, and $k_2 = 0{\cdot}0$. Figure 2 shows the field computed by a direct truncation of the series in Equation (15) with the truncation parameter

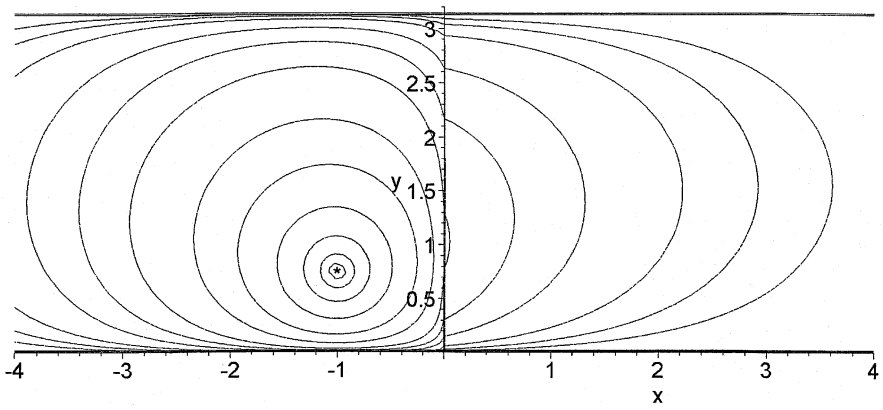

Figure 3. Smoothing attained by spliting off the singular component of the influence function.

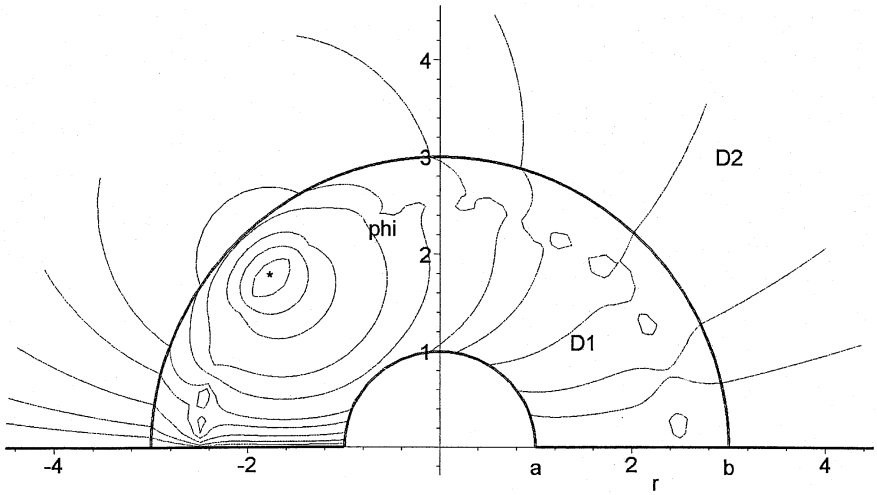

Figure 4. Profile of the influence function computed by truncation ($N = 20$) of its series representation.

$N = 20$, whereas the field depicted in Figure 3 was obtained by using Equations (19) and (20) where only the tenth partial sum was accounted for in the series expansions of the regular components. It is evident that the accuracy of the field shown in Figure 2 is unacceptably low, especially in a certain vicinity of the source point, whereas the splitting off of the singular terms radically eliminates the drawback.

Another illustration of the effect that is achieved by splitting off singular components of influence functions is given in Figures 4 and 5 (half-plane-shaped plate with a semi-circular cut-out). The problem setting assumes the Newtonian convection condition imposed on the contour of the cut-out. A pure series form, with the truncation parameter $N = 20$, is used in Figure 4, whereas Figure 5 shows the field computed with the singular components split off and the tenth partial sum accounted for in the series expansions of the regular components.

2.2. Semi-infinite strip-shaped plate

Consider a plate whose middle plane occupies the semi-infinite strip-shaped region $D = \{-a < x < \infty,\ 0 < y < b\}$ composed of the rectangular fragment $D_1 = \{-a < x < 0,\ 0 < y < b\}$ and the semi-strip $D_2 = \{0 < x < \infty,\ 0 < y < b\}$. The ideal thermal contact as simulated by

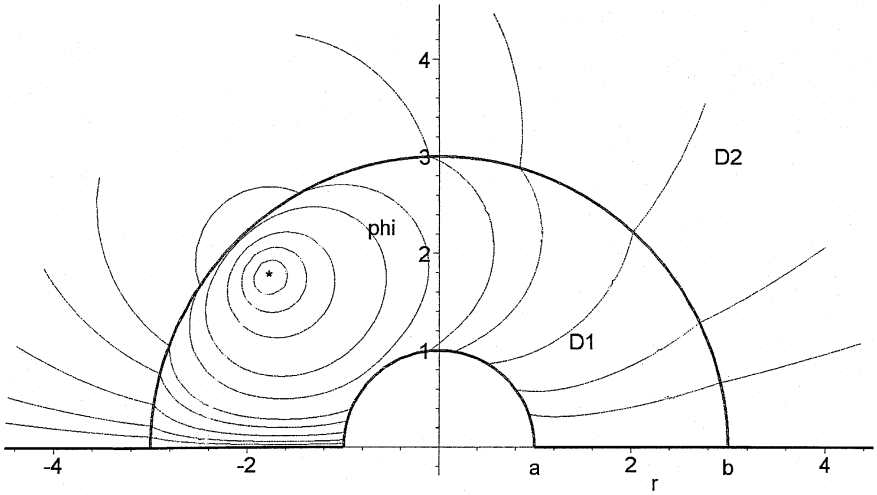

Figure 5. Smoothing delivered to the influence function by spliting off its singular component.

(3) is assumed on the interface $x = 0$, while boundary conditions on the edges $y = 0$, $y = b$, $x = -a$, and as x approaches infinity are given by

$$u_i(x, 0) = 0, \quad \frac{\partial u_i(x, b)}{\partial y} = 0, \quad (i = 1, 2), \tag{21}$$

$$\frac{\partial u_1(-a, y)}{\partial x} - \beta u_1(-a, y) = 0, \quad \beta \geq 0, \quad |u_2(\infty, y)| < \infty. \tag{22}$$

To find the solution to the problem defined by (3), (4), (21), and (22), the functions $u_i(x, y)$ and $f_i(x, y)$ are expanded in Fourier series as shown in (5) and (6) where, in this case, the summation parameter ν is defined as

$$\nu = \frac{(2n-1)\pi}{2b}, \quad i = 1, 2$$

satisfying the boundary conditions of (21).

With this, one arrives at the differential equation

$$\frac{\mathrm{d}^2 u_{1,n}(x)}{\mathrm{d}x^2} - (\nu^2 + k_1^2) u_{1,n}(x) = -f_{1,n}(x), \quad x \in (-a, 0) \tag{23}$$

for the coefficients $u_{1,n}(x)$ of the series in Equation (5), while the differential equation in (8) governs the coefficients $u_{2,n}(x)$. The boundary conditions of (22) result in

$$\frac{\mathrm{d}u_{i,n}(-a)}{\mathrm{d}x} - \beta u_{i,n}(-a) = 0, \quad |u_{2,n}(\infty)| < \infty \tag{24}$$

and the contact conditions in (3) reduce to those shown in (10).

Tracing out the procedure of Section 2.1, we obtain the solution to the boundary-contact-value problem as defined by (8), (10), (23), and (24) in the form

$$u_{1,n}(x) = \int_{-a}^{0} g_{11}^n(x, \xi) f_{1,n}(\xi) \mathrm{d}\xi + \int_0^{\infty} g_{12}^n(x, \xi) f_{2,n}(\xi) \mathrm{d}\xi$$

and

$$u_{1,n}(x) = \int_{-a}^{0} g_{21}^{n}(x,\xi)\, f_{1,n}(\xi)\mathrm{d}\xi + \int_{0}^{\infty} g_{22}^{n}(x,\xi)\, f_{2,n}(\xi)\mathrm{d}\xi,$$

where the kernel functions $g_{ij}^{n}(x,\xi)$ are found to be

$$g_{11}^{n}(x,\xi) = \frac{1}{2h_1\Delta}\left\{(h_1+\beta)\left[(h_1+\lambda h_2)\mathrm{e}^{-h_1|x-\xi|} + (h_1-\lambda h_2)\mathrm{e}^{h_1(x-\xi)}\right]\mathrm{e}^{2h_1 a}\right.$$

$$\left. +(h_1-\beta)\left[(h_1-\lambda h_2)\mathrm{e}^{h_1|x-\xi|} + (h_1+\lambda h_2)\mathrm{e}^{-h_1(x+\xi)}\right]\right\}, \tag{25}$$

with x and ξ belonging to the segment $[-a, 0]$,

$$g_{12}^{n}(x,\xi) = \frac{\lambda}{\Delta}\left[(h_1+\beta)\mathrm{e}^{h_1(x+2a)} + (h_1-\beta)\mathrm{e}^{-h_1 x}\right]\mathrm{e}^{-h_2\xi}, \tag{26}$$

with $x \in [-a, 0]$ and $\xi \in [0, \infty)$

$$g_{21}^{n}(x,\xi) = \frac{1}{\Delta}\left[(h_1+\beta)\mathrm{e}^{h_1(\xi+2a)} + (h_1-\beta)\mathrm{e}^{-h_1\xi}\right]\mathrm{e}^{-h_2 x}, \tag{27}$$

with $\xi \in [-a, 0]$ and $x \in [0, \infty)$, and

$$g_{22}^{n}(x,\xi) = \frac{1}{2h_2\Delta}\left\{(h_1+\beta)\left[(h_1+\lambda h_2)\mathrm{e}^{-h_2|x-\xi|} - (h_1-\lambda h_2)\mathrm{e}^{-h_2(x+\xi)}\right]\mathrm{e}^{2h_1 a}\right.$$

$$\left. -(h_1-\beta)\left[(h_1-\lambda h_2)\mathrm{e}^{-h_2|x-\xi|} - (h_1+\lambda h_2)\mathrm{e}^{-h_2(x+\xi)}\right]\right\}, \tag{28}$$

with x and ξ belonging to the segment $[0, \infty)$.

The parameter Δ in (25–28) is given as

$$\Delta = (h_1+\beta)(h_1+\lambda h_2)\mathrm{e}^{2h_1 a} + (h_1-\beta)(h_1-\lambda h_2).$$

This leads finally to the solution of the original boundary-contact-value problem posed by (3), (4), (21), and (22), as expressed in the form

$$u_i(x,y) = \int_0^{\pi}\int_{-a}^{0} G_{i1}(x,y;\xi,\eta)\, f_1(\xi,\eta)\mathrm{d}\xi\,\mathrm{d}\eta$$

$$+ \int_0^{\pi}\int_{0}^{\infty} G_{i2}(x,y;\xi,\eta)\, f_2(\xi,\eta)\mathrm{d}\xi\,\mathrm{d}\eta, \quad (x,y)\in D_i, \quad i=1,2,$$

where the kernel functions are given by

$$G_{ij}(x,y;\xi,\eta) = \frac{2}{b}\sum_{n=1}^{\infty} g_{ij}^{n}(x,\xi)\sin(\nu y)\sin(\nu\eta), \qquad \nu = \frac{(2n-1)\pi}{2b}, \tag{29}$$

with $g_{ij}^{n}(x,\xi)$, $(i, j = 1, 2)$ given by (25–28). This represents the influence function of a point source for the plate under consideration. As to the singular components of the diagonal entries $G_{11}(x,y;\xi,\eta)$ and $G_{22}(x,y;\xi,\eta)$, they can be split off in a manner similar to that

used in Section 2.1.1, which makes the above representation readily usable for computer implementations.

Influence functions of a point source, which have been or might be obtained by the technique proposed in this study, are helpful in solving various settings in thermal science. In the next section we discuss some of such statements for perforated plates. Another opportunity of utilization of influence functions is associated with a setting where a finite set of heat sources are acting simultaneously.

Consider again the plate composed of the fragments $D_1 = \{-a < x < 0,\ 0 < y < b\}$ and $D_2 = \{0 < x < \infty,\ 0 < y < b\}$. Let a finite number m_1 of sources of intensities $K_j^{(1)}$ be in action at points $(\xi_j, \eta_j) \in D_1$, with $j = \overline{1, m_1}$, while a finite number m_2 of sources of intensities $K_j^{(2)}$ are acting at points $(\xi_j, \eta_j) \in D_2$, with $j = \overline{1, m_2}$.

By the superposition principle, the aggregate field $W_1(x, y)$ generated in D_1 by all the point sources is, in this case, defined as

$$W_1(x, y) = \sum_{j=1}^{m_1} K_j^{(1)} G_{11}(x, y; \xi_j, \eta_j) + \sum_{j=1}^{m_2} K_j^{(2)} G_{12}(x, y; \xi_j, \eta_j),$$

while for the aggregate field $W_2(x, y)$ generated in D_2, we have

$$W_2(x, y) = \sum_{j=1}^{m_1} K_j^{(1)} G_{21}(x, y; \xi_j, \eta_j) + \sum_{j=1}^{m_2} K_j^{(2)} G_{22}(x, y; \xi_j, \eta_j),$$

where the kernel functions $G_{ij}(x, y; \xi, \eta)$ are defined by Equation (29). In Section 3.1 we demonstrate practical aspects of using this algorithm for computing thermal fields generated with multiple point sources in compound plates which, in addition, are weakened by apertures.

3. Perforated plates

The purpose in this section is to develop a numerical procedure for computing thermal fields generated by either point sources in compound plates weakened by apertures or by some non-zero boundary conditions imposed on apertures, or even combinations of these. Matrices of Green's type previously constructed for solid compound plates of standard shape (of the kind that have been discussed in Section 2) will be used herein as a basis for the procedure.

We consider a compound plate with a middle plane occupying the semi-infinite strip-shaped region $D = D_1 \cup D_2$ considered in Section 2.2. The plate is weakened by an aperture of smooth contour L located in D_1, and is undergoing a point source of intensity K acting at $(x_0, y_0) \in D_2$ (see Figure 6). Note that the procedure to be developed is not limited to the above setting and such a specific location of the point source and the aperture are chosen just for the sake of fixing the presentation.

The boundary conditions on the outer contour of the plate are assumed to be those of (21) and (22), while the contact conditions on the material interface $x = 0$ are given by (3). The boundary condition on the edge L of aperture is imposed as

$$u_1(x, y) = 0, \quad (x, y) \in L. \tag{30}$$

Clearly, the thermal field generated in the plate by a point source is determined by the matrix of Green's type of the boundary-contact-value problem stated by the Equations (3),

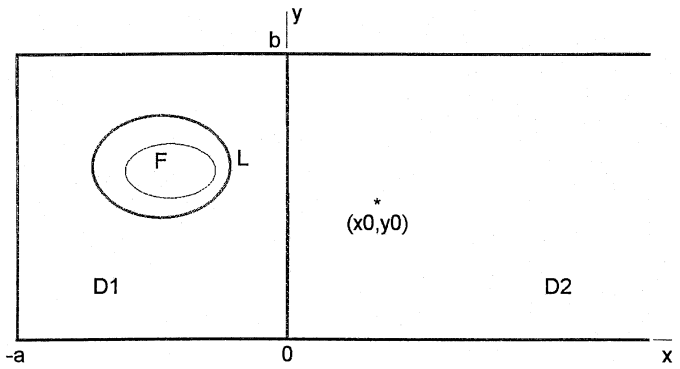

Figure 6. To the statement of the problem in Equations (3), (4), (21), (22), and (30).

(4), (21), (22), and (30). Since the source point is, in this setting, placed in D_2, the second column

$$\left(\widetilde{G}_{12}(x, y; x_0, y_0)\ \widetilde{G}_{22}(x, y; x_0, y_0)\right)^T$$

of that matrix is the one that should be looked for and we express it in the form

$$\begin{pmatrix}\widetilde{G}_{12}(x, y; x_0, y_0)\\ \widetilde{G}_{22}(x, y; x_0, y_0)\end{pmatrix} = K\begin{pmatrix}G_{12}(x, y; x_0, y_0)\\ G_{22}(x, y; x_0, y_0)\end{pmatrix} + \begin{pmatrix}g_{12}(x, y)\\ g_{22}(x, y)\end{pmatrix}, \tag{31}$$

where $G_{12}(x, y; x_0, y_0)$ and $G_{22}(x, y; x_0, y_0)$ are the entries of the second column of the matrix of Green's type that is defined by (29).

From (31), it follows that the regular components $g_{12}(x, y)$ and $g_{22}(x, y)$ ought to be solutions of the homogeneous equations corresponding to those in (4), and have to satisfy the following boundary and contact conditions

$$g_{i2}(x, 0) = 0, \quad \frac{\partial g_{i2}(x, b)}{\partial y} = 0, \quad (i = 1, 2), \tag{32}$$

$$\frac{\partial g_{12}(-a, y)}{\partial x} - \beta g_{12}(-a, y) = 0, \quad |g_{22}(\infty, y)| < \infty, \tag{33}$$

$$g_{12}(0, y) = g_{22}(0, y), \quad \frac{\partial g_{12}(0, y)}{\partial x} = \lambda\frac{\partial g_{22}(0, y)}{\partial x}, \tag{34}$$

$$g_{12}(x, y) = -KG_{12}(x, y; x_0, y_0), \quad (x, y) \in L. \tag{35}$$

We express $g_{12}(x, y)$ and $g_{22}(x, y)$ by means of the single-layer-type potential representation

$$\begin{pmatrix}g_{12}(x, y)\\ g_{22}(x, y)\end{pmatrix} = \int_F \mu(\xi, \eta)\begin{pmatrix}G_{11}(x, y; \xi, \eta)\\ G_{21}(x, y; \xi, \eta)\end{pmatrix} \mathrm{d}F(\xi, \eta), \tag{36}$$

where the density function $\mu(\xi, \eta)$ has yet to be found. The integration line F in (36) is a smooth closed curve which entirely belongs to the interior of L (see Figure 6) and is referred to herein as the *fictitious contour*.

Inasmuch as the kernel of the representation in (36) consists of the entries of the matrix of Green's type given by (29), the functions $g_{12}(x, y)$ and $g_{22}(x, y)$ satisfy the relations in (32–34). And, since the aperture L is located in D_2, the boundary condition of (35) results in the following functional (integral type) equation

$$-KG_{12}(x, y; x_0, y_0) = \int_F G_{11}(x, y; \xi, \eta)\mu(\xi, \eta)\mathrm{d}F(\xi, \eta), \quad (x, y) \in L \tag{37}$$

in the density function $\mu(\xi, \eta)$. As to a numerical solution of this equation, it has to be pointed out that the set of integration points $(\xi, \eta) \in F$ is different from the set of field points $(x, y) \in L$ in (37). This makes the kernel $G_{11}(x, y; \xi, \eta)$ a regular function and, thus, a numerical solution of Equation (37) should not be a problem for a fixed shape and position of the fictitious contour. The only concern that remains is how the spacing of F affects the accuracy level of the described procedure. Some specific suggestions on this and other important computational details in this procedure are addressed in the next section.

3.1. Validation problem and illustrative examples

To focus on numerical aspects of the algorithm and to find optimal values of its computational parameters, a validation problem is stated, namely one that allows an exact solution. That is, we consider the semi-infinite strip-shaped region D with an aperture as shown in Figure 6. Let the contour L be an ellipse defined as

$$\frac{(x - x_c)^2}{a_0^2} + \frac{(y - y_c)^2}{b_0^2} = 1 \tag{38}$$

and the boundary and contact conditions on the outer contour of D and on the material interface $x = 0$ be those defined by (3), (21), and (22), while the boundary condition on L be specified as

$$u_1(x, y) = \Psi(x, y), \quad (x, y) \in L. \tag{39}$$

It appears that we can readily formulate a validation problem for the setting in (3), (4), (21), (22), and (39). This can be done with the aid of the matrix of Green's type derived in (29). Indeed, it is evident that, if the right-hand side function $\Psi(x, y)$ in (39) represents the trace of the entry $G_{11}(x, y; x_0, y_0)$ of that matrix of Green's type, that is,

$$\Psi(x, y) = G_{11}(x, y; x_0, y_0), \quad (x, y) \in L,$$

with the source point (x_0, y_0) arbitrarily located inside the aperture, then the entries $G_{11}(x, y; x_0, y_0)$, with $(x, y) \in D_1$, and $G_{21}(x, y; x_0, y_0)$, with $(x, y) \in D_2$, represent the exact solution to the boundary-contact-value problem defined by (3), (4), (21), (22), and (39). This is true because the region D that we consider does not include the interior of L, where the source point is located (recall that the component $G_{11}(x, y; x_0, y_0)$ is not supposed to satisfy the governing equation (4) if (x, y) coincides with (x_0, y_0) which is not the case under the given circumstances).

In compliance with the algorithm proposed in Section 3, the approximate solution to the problem defined by (3), (4), (21),(22), and (39) is sought as

$$\begin{pmatrix} u_1(x, y) \\ u_2(x, y) \end{pmatrix} = \int_F \begin{pmatrix} G_{11}(x, y; \xi, \eta) \\ G_{21}(x, y; \xi, \eta) \end{pmatrix} \mu(\xi, \eta)\mathrm{d}F(\xi, \eta), \quad (x, y) \in D. \tag{40}$$

Table 1. Accuracy attained for the setting in Equations (3), (4), (21),(22), and (39).

Number M of quadrature nodes	x coordinate of the field point on the line $y = y_c$						
	$-2{\cdot}00$	$-1{\cdot}75$	$-1{\cdot}70$	$-0{\cdot}70$	$-0{\cdot}65$	$0{\cdot}00$	$1{\cdot}00$
10	0·08411	0·12721	0·14199	0·13247	0·11663	0·01543	0·00813
20	0·08603	0·12929	0·14199	0·13247	0·11865	0·01573	0·00827
30	0·08624	0·12973	0·14199	0·13247	0·11910	0·01576	0·00829
Exact value	0·08628	0·12986	0·14199	0·13247	0·11922	0·01576	0·00829

To find the density function $\mu(\xi, \eta)$ in the above potential, we take the limit in (40) as (x, y) approaches L. With this, we arrive at the following functional (of integral type) equation

$$G_{11}(x, y; x_0, y_0) = \int_F G_{11}(x, y; \xi, \eta)\mu(\xi, \eta)\mathrm{d}F(\xi, \eta), \quad (x, y) \in L \tag{41}$$

in $\mu(\xi, \eta)$.

So, once a numerical solution of (41) is obtained, approximate values of $u_1(x, y)$ and $u_2(x, y)$ can be computed by carrying out a numerical integration in (40). And this reveals the accuracy level provided by the algorithm, since the approximate solution that is so obtained can be compared with the exact one which is available in this case.

The standard trapezoidal rule, with M representing the number of quadrature nodes uniformly spaced on the fictitious contour F, has been used for computing the line integrals in (40) and (41). As our experience convincingly suggests, in finding an optimal shape and location of the regularizing contour F, we can limit ourselves to circles concentric with L. And this appears to be true for a broad range of aperture shapes.

Table 1 illustrates the accuracy level attained with our approach. We considered a setting in which the physical and geometrical parameters have been chosen as: $a = 3{\cdot}0$, $b = 3{\cdot}0$, $k_1 = 1{\cdot}0$, $k_2 = 0$, $\beta = 1{\cdot}0$, $\lambda = 10{\cdot}0$, $x_c = -1{\cdot}2$, $y_c = 1{\cdot}5$, $a_0 = 0{\cdot}5$, and $b_0 = 0{\cdot}7$. The optimal value R_0 of the radius of the fictitious contour F was found to be $R_0 = 0{\cdot}45$. Values of the approximate solution have been computed at a set of field points that are spaced in a nonuniform fashion on the line $y = y_c$ passing through the center of the aperture. We focused on the immediate vicinity of the aperture to find out if the accuracy is affected by the closeness of the field point to the aperture.

The most evident observations that follow from the data in Table 1 are:

(i) the optimal radius R_0 of the fictitious contour F is recommended to be at a level of about 90% of the minimal radius of aperture L;

(ii) the overall accuracy level increases notably when the number M of the quadrature nodes increases (compare the data by the rows);

(iii) the accuracy slightly drops as the field point approaches the contour L, remaining however relatively high (at about 0·1% level), even for the points closely located to L (observe the second and the fifth columns);

(iv) the accuracy reaches its highest overall level when the field point lies on L, even for the lowest number ($M = 10$) of the quadrature nodes.

Note that the last observation is not surprising; it follows from the nature of the algorithm, inasmuch as the Equation (41) emerges from the "exact" satisfaction of the boundary condition in (39).

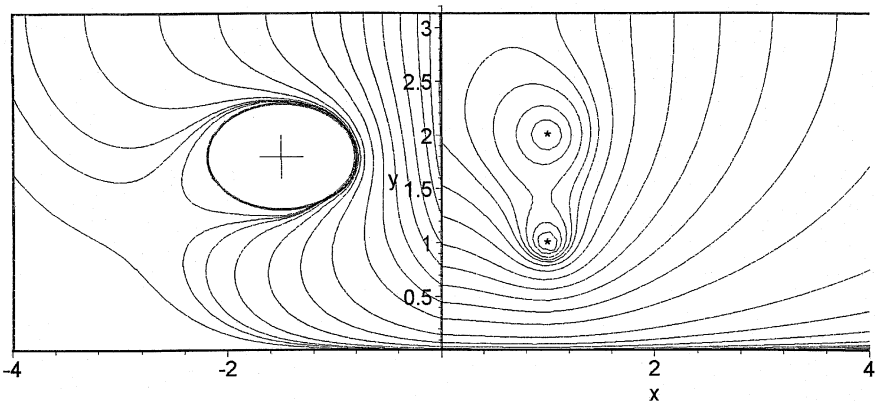

Figure 7. Thermal field generated by point sources in the compound plate having an aperture.

Recommendations about the key computational parameters (M and R_0) that follow from the above validation setting are helpful in solving other problems. Let us, for example, compute a potential field generated by a finite number of point sources in the compound plate whose middle plane is shown in Figure 6. Let the contour $L \in D_1$ of the aperture be specified by Equation (38) and m point sources of different intensities K_i be put at points (x_i, y_i) in D_2.

The algorithm proposed in Section 3 has been utilized for computing the field, with a few modifications. That is, the first additive component of (31) reads, in this case, as

$$\sum_{i=1}^{m} K_i \begin{pmatrix} G_{12}(x, y; x_i, y_i) \\ G_{22}(x, y; x_i, y_i) \end{pmatrix}.$$

The boundary condition of Equation (35) transforms into

$$g_{12}(x, y) = -\sum_{i=1}^{m} K_i G_{12}(x, y; x_i, y_i), \quad (x, y) \in L$$

and Equation (37) reads as

$$-\sum_{i=1}^{m} K_i G_{12}(x, y; x_i, y_i) = \int_F G_{11}(x, y; \xi, \eta)\mu(\xi, \eta)\mathrm{d}F(\xi, \eta), \quad (x, y) \in L.$$

Figure 7 depicts the field generated by two sources in the compound plate whose middle plane occupies the region $D = D_1 \cup D_2$ considered in Section 2.2. The intensities of sources are $K_1 = 3{\cdot}0$ and $K_2 = 2{\cdot}0$. The shape and location of the aperture are given as: $x_c = -1{\cdot}5$, $y_c = 1{\cdot}8$, $a_0 = 0{\cdot}7$, and $b_0 = 0{\cdot}5$. The rest of the parameters in the setting are: $a = 4{\cdot}0$, $b = \pi$, $k_1^2 = 0$, $k_2^2 = 1{\cdot}0$, $\beta = 1{\cdot}0$, $\lambda = 10{\cdot}0$, and $R_0 = 0{\cdot}45$. This example reveals the potential of the proposed algorithm in computing temperature fields generated by multiple heat sources in a compound perforated plate. Our experience in dealing with a variety of problem settings of the considered type indicates that sources of different intensities located in different fragments of a compound plate can be successfully treated with the proposed approach.

The field in Figure 8 is generated by three unit sources in the plate of half-plane shape consisting of two fragments $D_1 = \{0 < r < a, \ 0 < \phi < \pi\}$ and $D_2 = \{a < r < \infty, \ 0 < \phi < \pi\}$, each of which is filled in with a different isotropic homogeneous material and hosts an aperture. Dirichlet boundary conditions are imposed on the edge of the half-plane and on the

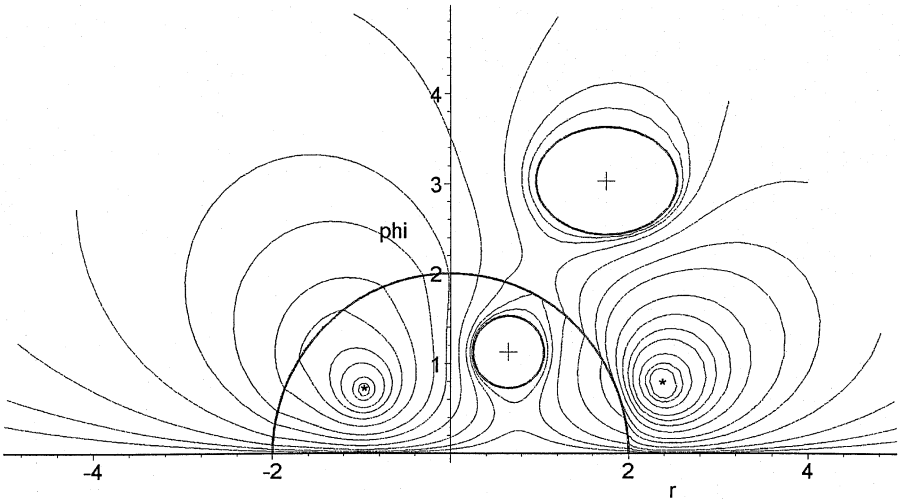

Figure 8. Point sources in a compound plate occupying half-plane and hosting two apertures.

contours of the apertures. The heat conductivity of the material of D_1 is ten times that of D_2 ($\lambda = 0{\cdot}1$). The matrix of Green's type for the solid compound half-plane plate, whose entries were used as kernels of an integral representation of the solution for the perforated plate, has been constructed with aid of the technique described in [2, Chapter 7].

We complete this presentation by demonstrating the use of influence functions computed herein in determining temperature fields that occur in a perforated compound plate and are generated not necessarily by point sources but rather by some nonzero boundary conditions imposed on the apertures contours.

Let the compound plate as considered in Section 2.2 be weakened by two apertures ($L_1 \in D_1$ and $L_2 \in D_2$) subject to the boundary conditions

$$u_1(x, y) = T_1, \ (x, y) \in L_1 \quad \text{and} \quad u_2(x, y) = T_2, \ (x, y) \in L_2$$

and let the plate's edges $x = -a$, $y = 0$, $y = b$ and the material interface $x = 0$ be subject to the boundary and the ideal contact conditions of (21), (22) and (3). The temperature field in the plate is expressed in the potential form

$$u_i(P) = \int_{F_1} G_{i1}(P; Q)\mu_1(Q)\mathrm{d}F_1(Q) + \int_{F_2} G_{i2}(P; Q)\mu_2(Q)\mathrm{d}F_2(Q), \ P \in D_i, i = 1, 2$$

with the kernel functions $G_{ij}(P; Q)$ being defined by (29). Upon satisfying the boundary conditions imposed on L_1 and L_2, one arrives at a system of functional equations in the densities $\mu_1(Q)$ and $\mu_2(Q)$ of the above potential.

In Figure 9, the field is shown as computed for the plate weakened by two congruent elliptic apertures that are symmetrically spaced about the material interface $x = 0$, with the following set of initial data applied: $a = 4{\cdot}0$, $b = \pi$, $k_1^2 = 1{\cdot}0$, $k_2^2 = 1{\cdot}0$, $\beta = 2{\cdot}0$, $\lambda = 0{\cdot}1$, $T_1 = 100$ and $T_2 = 150$.

From our experience in solving the problem class considered in this study, it follows that aperture configurations, their sizes, number and locations along with spacing and intensities of heat sources do not represent limiting factors in the proposed algorithm. As to shapes and locations of fictitious contours, we have found that in most cases these could be fixed as circles

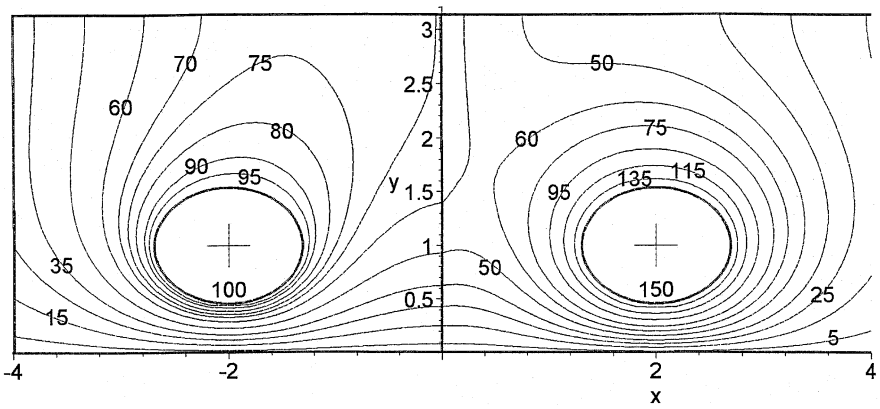

Figure 9. Semi-strip-shaped compound plate with apertures.

concentric with the contours of apertures, while their optimal radii are about $0{\cdot}90 - 0{\cdot}95$ of the smallest radius of the actual aperture.

4. Closing remarks

This project further extends the application area of influence functions in thermal sciences. It has been motivated by the creative potential that influence functions bring to both theory and practice. The study has primarily been aimed at:
(i) extension of our earlier elaborations on analytical construction of influence functions of a point source to plates of standard shape made of materials with piecewise constant physical properties and experiencing Newtonian convection through facial surfaces;
(ii) development of effective numerical procedures for computing influence functions for plates of standard configuration, but containing apertures making pure analytical approach problematic if not impossible;
(iii) demonstration of the computational potential of influence functions in solving applied problems in thermal sciences.

The study builds up a confidence in the constructive nature of the proposed representations of influence functions of a point source and suggests further ways of their effective utilization in thermal sciences. Some nonlinear problems, for example, or some classes of inverse formulations can be targeted, for which the availability of fast and accurately computable influence functions of the corresponding linear or direct formulations is absolutely crucial.

References

1. J.V. Beck, K.D. Cole, A. Haji-Sheikh and B. Litkouhi, *Heat Conduction Using Green's Functions.* New York: Hemisphere (1992) 550pp.
2. Yu.A. Melnikov, *Influence Functions and Matrices.* New York - Basel: Marcel Dekker (1999), 469pp.
3. J.C.F. Telles and S. Guimaraes, Green's function: a numerical generation for fracture mechanics problems via boundary elements. *Comp. Meth. Appl. Mech. Engng.* 188 (2000) 847–858.
4. D. Duffy, *Green's Functions with Applications.* Boca Raton: CRC Press (2001) 443pp.
5. J.R. Berger and V.K. Tewary, Green's functions for boundary element analysis of anisotropic materials. *Engng. Anal. Bound. Elem.* 25 (2001) 279–288.
6. B. Yang and E. Pan, Efficient evaluation of three-dimensional Green's function in anisotropic eleastostatic multilayered material composite. *Engng. Anal. Bound. Elem.* 26 (2002) 355–366.

7. V.I. Smirnov, *A Course of Higher Mathematics*, Vol. 4. Oxford - New York: Pergamon Press (1964) 812pp.
8. I.M. Dolgova and Yu.A. Melnikov, Construction of Green's functions and matrices for equations and systems of elliptic type. *J. Appl. Math. Mech.* 42 (1978) 740–746.
9. Yu.A. Melnikov, Accuracy of series approximations of Green's functions. In: *Int. Symp. Bound. Elem. Meth.* Paris (1998) 147–148.
10. S.L. Marshall, A rapidly convergent modified Green's function for Laplace equation in a rectangular region. *Proc. R. Soc. London* 455 (1999) 1739–1766.
11. G.F. Roach, *Green's Functions.* New York: Cambridge University Press (1982) 325pp.